Contents lists available at ScienceDirect

CARBON

journal homepage: www.elsevier.com/locate/carbon

Direct observation of electron emission from grain boundaries in CVD diamond by PeakForce-controlled tunnelling atomic force microscopy

CrossMark

Robert L. Harniman [a,*], Oliver J.L. Fox [a], Wiebke Janssen [b,c], Sien Drijkoningen [b], Ken Haenen [b,c], Paul W. May [a,*]

[a] School of Chemistry, University of Bristol, Cantock's Close, Bristol BS8 1TL, United Kingdom
[b] Institute for Materials Research (IMO), Hasselt University, Wetenschapspark 1, B-3590 Diepenbeek, Belgium
[c] IMOMEC, IMEC vzw, Wetenschapspark 1, B-3590 Diepenbeek, Belgium

A R T I C L E   I N F O

A B S T R A C T

A detailed investigation of electron emission from a set of chemical vapour deposited (CVD) diamond films is reported using high-resolution PeakForce-controlled tunnelling atomic force microscopy (PF-TUNA). Electron field emission originates preferentially from the grain boundaries in low-conductivity polycrystalline diamond samples, and not from the top of features or sharp edges. Samples with smaller grains and more grain boundaries, such as nanocrystalline diamond, produce a higher emission current over a more uniform area than diamond samples with larger grain size. Light doping with N, B or P increases the grain conductivity, with the result that the emitting grain-boundary sites become broader as the emission begins to creep up the grain sidewalls. For heavy B doping, where the grains are now more conducting than the grain boundaries, emission comes from both the grain boundaries and the grains almost equally. Lightly P-doped diamond samples show emission from step-edges on the (1 1 1) surfaces. Emission intensity was time dependent, with the measured current dropping to ~10% of its initial value ~30 h after removal from the CVD chamber. This decrease is ascribed to the build-up of adsorbates on the surface along with an increase in the surface conductivity due to surface transfer doping.

1. Introduction

Polycrystalline diamond films deposited by chemical vapour deposition (CVD) are excellent materials for use as electron field emitters due to their low or negative electron affinity (NEA), which lowers the effective surface potential barrier that electrons must overcome to escape into vacuum [1]. Furthermore, diamond has excellent chemical and mechanical properties, such as high hardness, very high thermal conductivity, and dopant-controlled electrical conductivity from highly insulating to near metallic, depending on the nature and concentration of the chosen dopant. These properties, together with its compatibility with silicon fabrication processes, make CVD diamond a potential candidate for a range of vacuum microelectronic devices, including high-power switches, electron sources/guns (for microwave tubes or high-definition television), high-speed and high-power amplifiers, integrated circuits [2], radio-frequency electron injectors [3] and

cathodes for photoinjectors [4]. Recently, we reported that applying a thin CVD diamond coating onto vertically aligned carbon nanotube (CNT) 'teepee' structures greatly extended the lifetime of field emission devices such that these structures might be used as field emitter arrays in commercial flat-panel displays [5].

However, the mechanism for electron emission from diamond remains unclear. Extraction of electrons from a diamond surface via application of a large applied electric field (field emission) generally follows the Fowler–Nordheim equation, Eq. (1), which was originally devised for electron emission from metals by quantum mechanical tunnelling through a potential barrier [6].

$$J(E) = \frac{A(\beta E)^2}{\phi} \exp\left(-\frac{b\phi^{3/2}}{\beta E}\right) \qquad (1)$$

Here, J ($A\,\mu m^{-2}$) is the emission current density at an applied electric field, E ($V\,\mu m^{-1}$), ϕ (eV) is the work function of the material, while A and b are material parameters with $b = 6.83 \times 10^3\,eV^{-3/2}\,V\,\mu m^{-1}$ and $A = 1.56 \times 10^{-6}\,A\,V^{-2}\,eV$. β is the 'field enhancement factor' which is usually interpreted as a geometrical effect due to sharp points or edges that concentrate the electric field. In order to increase the value of β and thereby

* Corresponding authors.
E-mail addresses: Rob.Harniman@bristol.ac.uk (R.L. Harniman), Paul.May@bristol.ac.uk (P.W. May).
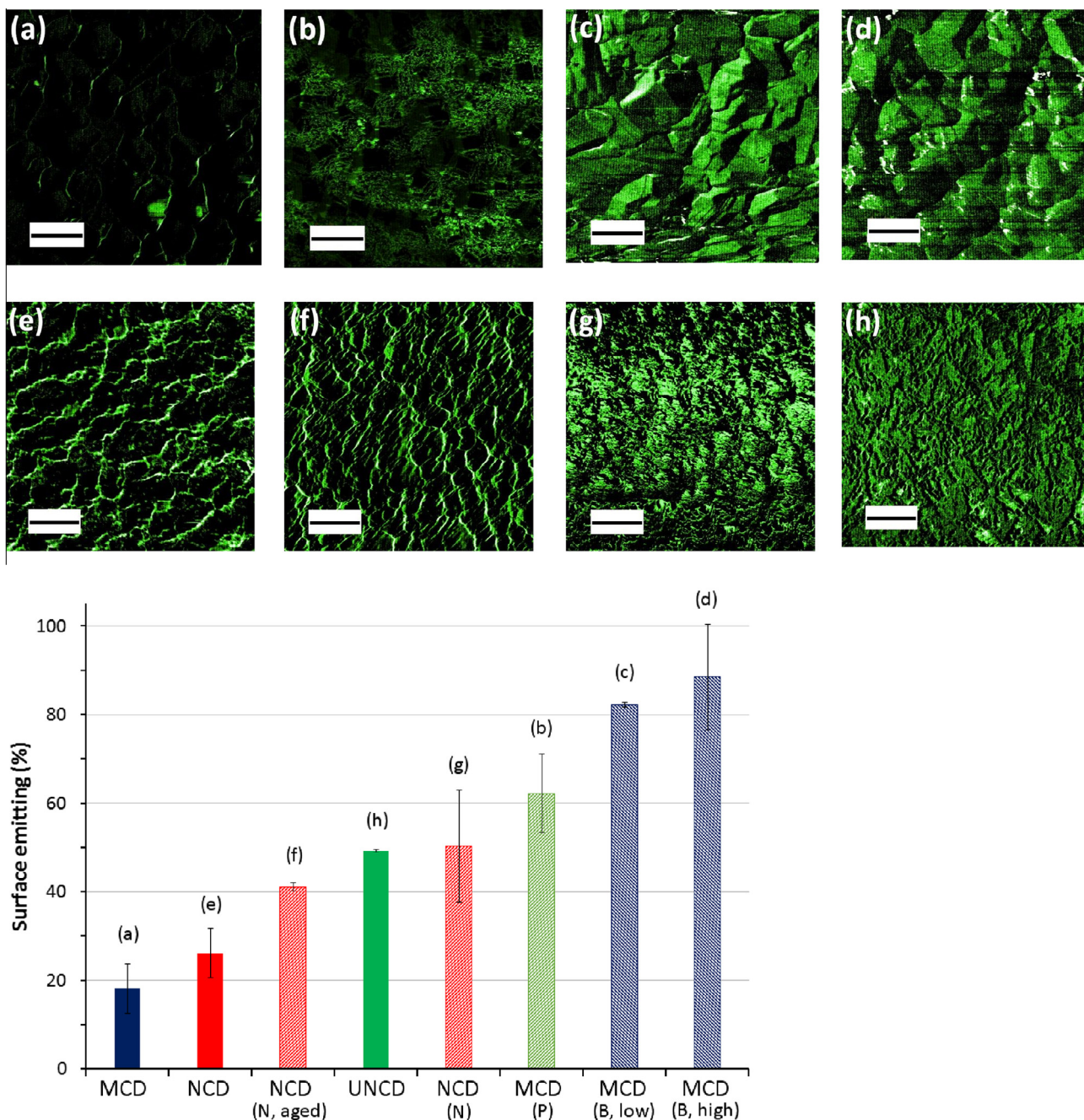
Fig. 1. Images of electron emission measured above CVD diamond samples (a) MCD, (b) phosphorus-doped MCD, (c, d) MCD with low and high levels of boron doping, respectively, (e) NCD, (f, g) NCD doped with nitrogen after >800 h removal from the reactor and 5 h, respectively, (h) UNCD. The brightness at any point in the images is proportional to the electron emission intensity at that point. Grain boundaries are clear as emission sites in all images except from the boron-doped samples that emit across whole grains but with varying intensity from different facets. Scale bars represent 1 μm except for (f) where it represents 0.5 μm. Below is a bar-chart of the associated percentage of each sample (a–h) measured to be emitting electrons above a threshold set at the r.m.s. current.

improve the emission efficiency, considerable effort has been spent by many research groups to process diamond into needles, cones, pyramids or other sharp-tipped structures [1]. However, the β values reported from diamond and other carbon surfaces are often in the range of 1000–10,000, significantly higher than the values of 10–100 resulting from theoretical consideration of geometrical effects alone [7]. Furthermore, studies using CNTs have shown that short, stubby CNTs [8], or extremely short CNTs [9], field-emit electrons more efficiently than longer ones, inconsistent with conventional ideas.

To explain these discrepancies, a number of other mechanisms have been proposed for the field enhancement. Geis et al. [10] suggested that field enhancement occurs at the triple junction between the diamond film, the substrate and vacuum. In this model, electrons tunnel from the substrate into diamond surface states, and are then accelerated by the applied field, usually traveling through grain boundaries or up the sides of diamond grains, to the surface where they are emitted into vacuum. However, this mechanism does not account for enhanced field emission from very thick diamond samples (where the field at the base of the film
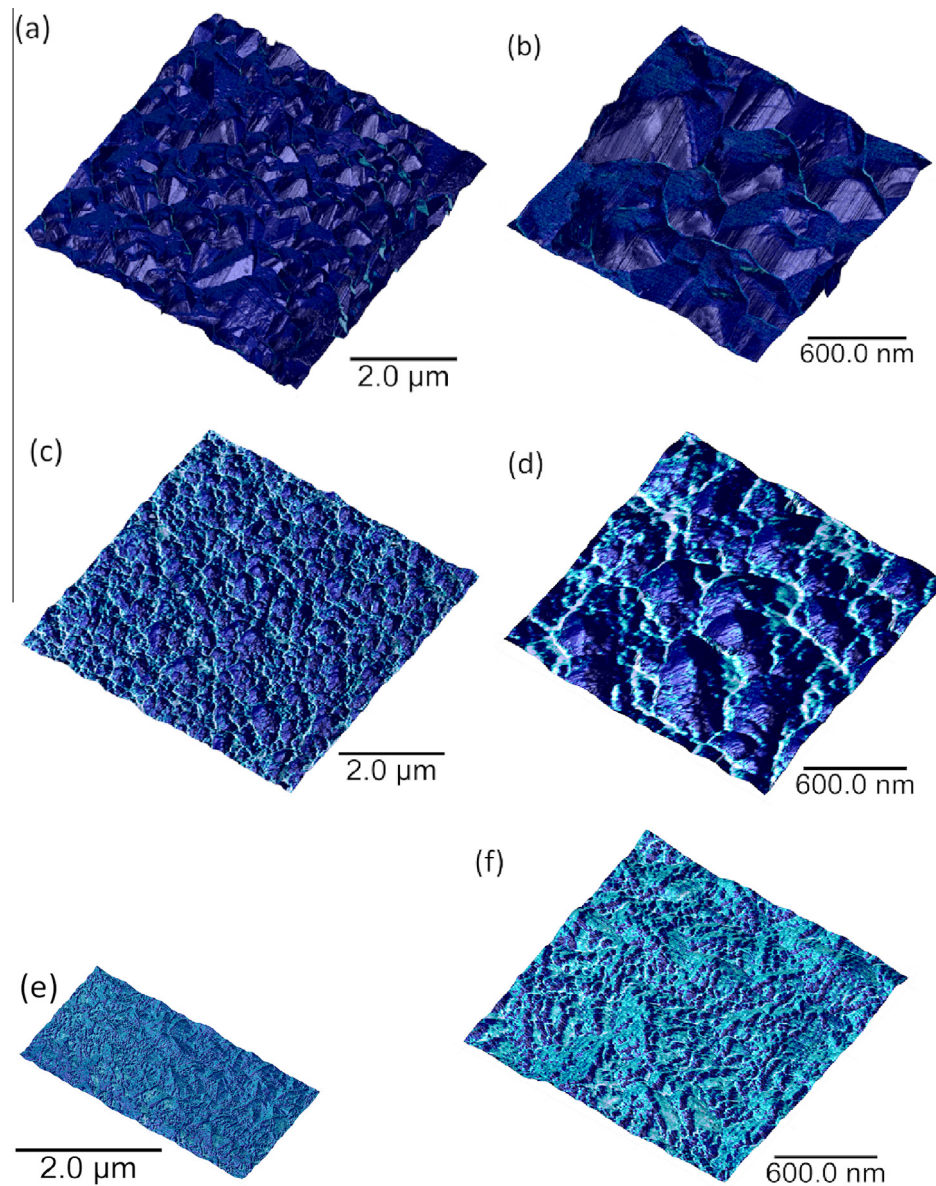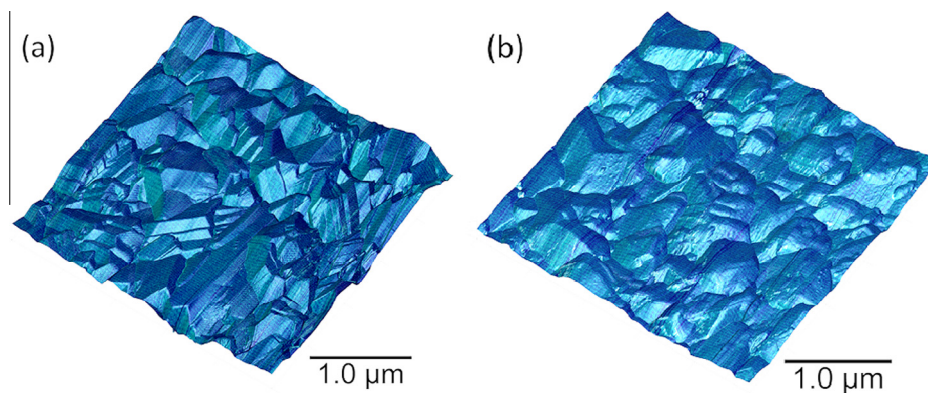
Fig. 2. Measured emission current overlaid on their corresponding measured topographic image for (a, b) undoped MCD, (c, d) undoped NCD, and (e, f) undoped UNCD samples. The images have been colour-scaled from dark–blue (low emission) to light–blue (high emission). The left-hand images (a, c, e) are large-area scans (a, c) 10 μm × 10 μm, (e) 10 μm × 5 μm, while the right-hand images (b, d, f) are images of smaller regions (3 μm × 3 μm) revealing more detail of the grain structure. Electron emission is evident from grain boundaries at all grain sizes. Higher resolution versions of these images can be found in the Supplementary Material. (For interpretation of the references to colour in this figure legend, the reader is referred to the web version of this article.)

is very small) or from freestanding diamond films where there is no substrate and hence no triple junction.

Experiments have shown that a hydrogenated polycrystalline diamond surface is necessary to obtain high electron yields [11]. The electron emission seems to correlate with the number and density of grain boundaries containing non-diamond sp^2 carbon [12]. Indeed, single-crystal diamond shows little, if any, field emission. To explain this, Cui et al. [13] devised a mechanism where the threshold for field emission is lowered due to a local reduction of the electron affinity of the diamond surface surrounding nanoscale graphitic surface structures, such as defects or grain boundaries. Electron emission actually takes place from the graphitic region, but the emission barrier is controlled by the surrounding diamond lattice. A similar model accounting for the enhanced field emission from other forms of carbon samples, including flat, smooth diamond-like carbon, was suggested by Robertson [14] and by

Ilie and co-workers [15]. These models are backed up by some experimental evidence. For instance, enhanced field emission was observed from a diamond surface when it was deliberately covered with nanoscale patches of graphitic impurities [16]. Likewise, when undoped polycrystalline and single-crystal diamond particles were deposited onto Si samples, only the samples covered with polycrystalline particles exhibited electron emission. Miyamoto et al. [17] showed theoretically that the potential profile at the surface strongly affects the emission efficiency, and that this could be modified based on the local surface geometry. Nitrogen-doped ultrananocrystalline diamond (UNCD) samples deposited on a flat surface also exhibit low threshold electric fields; this provides strong evidence that sub-nm-sized grain boundaries might enhance the local electric fields as effectively – or even more effectively – than sharp features [18]. To test this idea, May et al. [19] deliberately used excessive bias to burn out the emission sites

Fig. 3. Measured emission current overlaid on their corresponding measured topographic image for boron-doped MCD samples at a scale of 5 μm × 5 μm with (a) low doping and (b) high doping. The images have been colour-scaled from dark–blue (low emission) to light–blue (high emission). Higher resolution versions of these images can be found in the Supplementary Material. (For interpretation of the references to colour in this figure legend, the reader is referred to the web version of this article.)
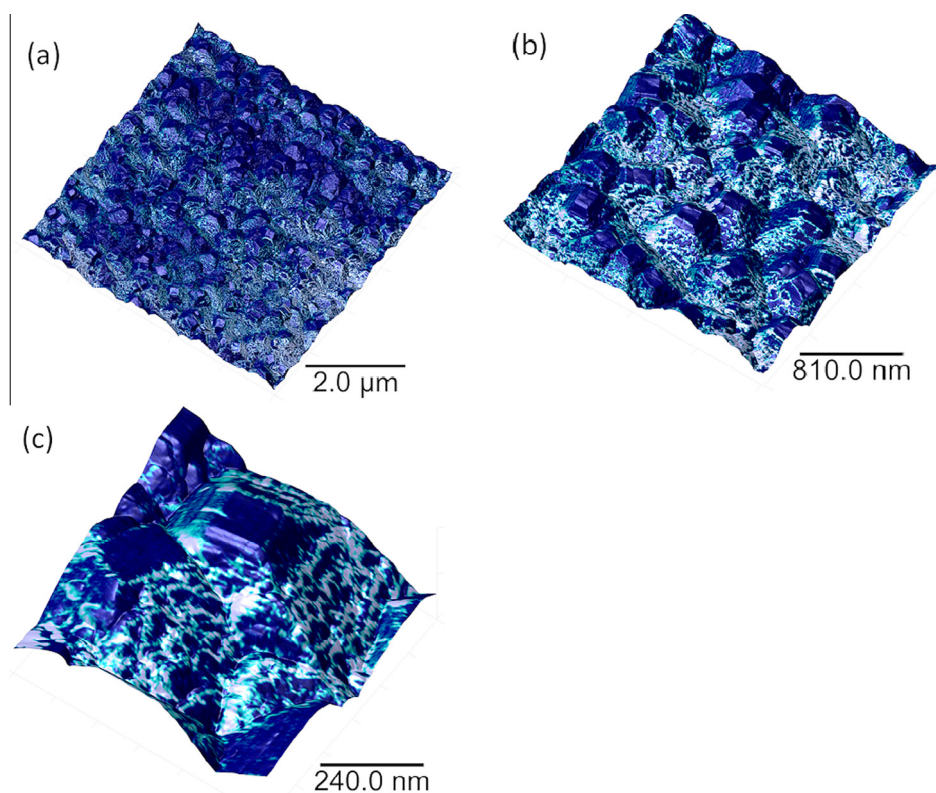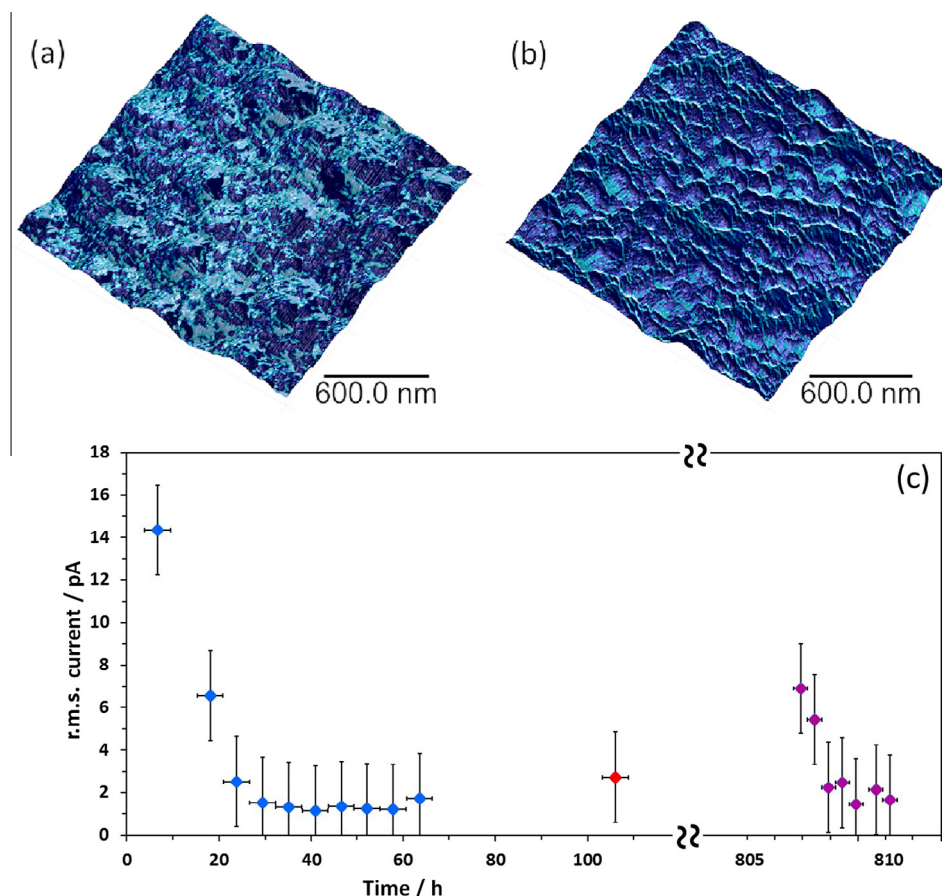
Fig. 4. Measured emission current overlaid on their corresponding measured topographic image of a phosphorus-doped MCD sample, at three levels of magnification: (a) 10 μm × 10 μm, (b) 4 μm × 4 μm, (c) 1.2 μm × 1.2 μm. The images have been colour-scaled from dark–blue (low emission) to light–blue (high emission). Higher resolution versions of these images can be found in the Supplementary Material. (For interpretation of the references to colour in this figure legend, the reader is referred to the web version of this article.)

on polycrystalline diamond surfaces. Imaging of the damage sites revealed ring-like craters surrounding intact grains, suggesting that the grain boundary, not the tip of the grain, had been eroded away by the excessive current.

Despite this circumstantial evidence, direct confirmation of grain-boundary emission has proven elusive. Field electron emission microscopy (FEEM) has the potential to image and determine the origin of field-emitted electrons from polycrystalline diamond. Unfortunately, FEEM has proved to be difficult to implement on diamond surfaces, with insufficient resolution to accurately determine the emission sites. The authors of a FEEM study of the emitting sites on nanocrystalline diamond films [20] concluded that the emission originated from localized regions smaller than 100 nm in size, but they could not say for certain if these were from grain boundaries.

Three reports have arguably provided the most convincing direct evidence for grain-boundary emission to date. They describe the use of scanning tunnelling microscopy (STM) to simultaneously map the morphology and field emission intensity of diamond surfaces. STM was first used to study a microcrystalline diamond surface as early as 1999 [21], and showed that the emission sites seemed to be associated with the valleys between grains and not with any sharp tips. However, due to the limitations of STM technology at that time, data for only one sample at 400 nm × 400 nm

Fig. 5. Measured emission current overlaid on corresponding measured topographic image (3 × 3 µm) for a nitrogen-doped NCD sample. (a) 5 h after removal from the reactor. (b) 810 h after removal from the MWCVD reactor. The images have been colour-scaled from dark–blue (low emission) to light–blue (high emission). The lower brightness of (b) compared to (a) indicates that the emission intensity has substantially decreased over this time period. High resolution versions of these images can be found in the Supplementary Material. (c) The measured electron emission current from the same region of the sample as a function of time after removal from the reactor. The first current measurement was made 5 h after deposition, with the sample remaining under ambient conditions in the PF-TUNA apparatus for subsequent measurements up to 65 h. The point marked in red represents a scan taken after 105 h in a different region of the sample (after the sample had been removed from the PF-TUNA apparatus and then replaced) to ensure that the reduction in emission was not induced by degradation of the tip. After 805 h the sample was baked in an oven at 200 °C for 2 h to desorb surface adsorbates. The emission current was then remeasured using PF-TUNA every ∼30 min until the value levelled off. Note the change in horizontal scale on the right-hand section of the plot. (For interpretation of the references to colour in this figure legend, the reader is referred to the web version of this article.)

resolution was presented. One of the most detailed scanning-probe studies of surface emission was performed by Krauss et al. in 2001 [22] who used a metal-coated atomic force microscope (AFM) tip in contact with the surface of a UNCD-coated Si micro-emitter to measure the surface topography. Applying electric fields to the AFM tip allowed them to measure the contact current at different locations. Results showed that the current was correlated with re-entrant cavities in the surface topography, *i.e.* to the valleys not the peaks. The authors concluded that the grain boundaries provided a conducting path from the substrate to the surface as well as enhancing the local electric field. More recently, another group has employed a high-resolution STM technique to study 'Cu-doped' [23] and Pt-implanted [24] UNCD samples. They also reported that the grain boundaries were the main emission sites, and showed current–voltage emission characteristics that were far superior for the grain boundary regions compared to those for the grains. The incorporation of Cu or Pt was necessary to make the UNCD samples conducting enough to obtain a measureable tunnelling current. However, the unknown position and nature of the metal in these samples (which probably is not a dopant in the true electronic sense, but conducting nanoparticles residing in the grain boundaries), makes the results difficult to relate to more conventional diamond samples.

Over the past few years, advances in both STM and AFM equipment and techniques have enabled the development of a hybrid of conducting-AFM-STM into a highly sensitive technique called tunneling atomic force microscopy [25], which has been given the official designation 'TUNA' by the equipment manufacturers (Bruker). TUNA allows a tunnelling current to be obtained from a nanosharp tip attached to a cantilever while simultaneously moving the tip across the sample surface to measure topographical data. In contrast to standard STM which requires sample surfaces to be smooth on the nanometer scale, TUNA can investigate surfaces with an r.m.s. roughness of several microns. Moreover, the surface can be studied over scan areas up to hundreds of square microns, allowing a wider picture of the overall morphology to be obtained. Furthermore, unlike the constant-current mode of STM, the physical tracking of TUNA means that the height data collected from the deflection of the cantilever avoids possible artefacts introduced by variations in the conductivity of the sample surface. Another major advantage of TUNA is that it has very high current sensitivity with a noise level of 50 fA. For the first time this permits the characterisation of low-conductivity diamond samples at high lateral resolution.

In this study, TUNA is combined with a sensitive feedback control mechanism, called PeakForce by the manufacturers (Bruker,
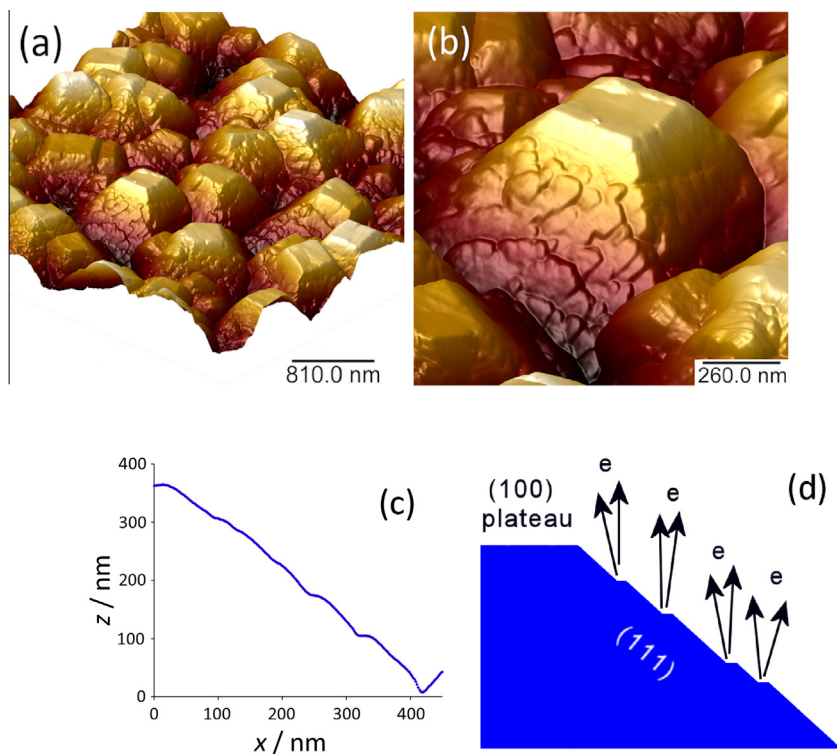
Fig. 6. (a, b) High-resolution AFM topography scans of the P-doped MCD film shown in Fig. 4 at two magnifications. The nanoscale steps can be seen on the (1 1 1) faces (slightly rounded due to convolution with the AFM tip). The images have been colour-shaded for height in the vertical z-direction. (c) AFM line profile up the (1 1 1) face of the central grain shown in (b), with x being the horizontal distance and z the vertical distance, showing clearly the stepped structure on the face – slightly rounded as before due to tip convolution. (d) Schematic diagram for the proposed model for electron emission from P-doped MCD. No emission is observed from the (1 0 0) plateaus, nor from the (1 1 1) terraces. Instead emission probably originates from nanoscale step-edges along the (1 1 1) surface, where the local electric field is enhanced by a similar mechanism to that proposed at grain boundaries. (For interpretation of the references to colour in this figure legend, the reader is referred to the web version of this article.)

CA, USA), that maintains an air gap between the AFM tip and the sample across which emitted electrons must travel. PeakForce is a non-harmonic feedback system in which force curves are taken regularly along a scan-line allowing the feedback parameter – the interaction force between the tip and the sample surface – to be maintained at a set-point. Specifying a force level <1 nN as the set-point ensures that tip-sample interaction remains in the weakly attractive region of the Lennard-Jones potential [26] with a separation of ~1 nm. Imaging in the attractive potential is well established in the field of non-contact AFM [27], where low-amplitude harmonic oscillation of stiff cantilevers, particularly in UHV environments, has allowed atomic and sub-atomic resolution [28] to be achieved. With non-harmonic PeakForce control, the necessary force level, and therefore separation, can be maintained more directly, allowing PeakForce-TUNA (PF-TUNA) measurements and surface topography to be collected simultaneously in a non-contact regime.

Recently, our group reported the first, low-resolution, PF-TUNA investigations of polycrystalline diamond surfaces [29]. This technique allowed the first direct observation of grain-boundary emission from undoped CVD diamond samples, and provided supporting evidence of the emission mechanism described in Cui et al. [13]. Having perfected the PF-TUNA technique, we now revisit these studies in higher resolution, and also study the effects of p- and n-type dopants on the field emission sites.

2. Experimental

2.1. CVD diamond sample fabrication

A set of diamond film samples was deposited on 1 cm^2 Si (1 0 0) substrates that had been pre-seeded with a suspension of 5–10 nm nanodiamond, either by electrospraying [30] or by dipping and spinning [31]. Different growth conditions were used to prepare samples with varying crystallite size, surface morphology and doping level.

2.1.1. Undoped microcrystalline diamond (MCD)

These samples were deposited using a microwave plasma CVD (MWCVD) reactor operating at 1.0 kW power and 125 torr, using 4.4%CH$_4$/7%Ar/H$_2$ process gases, at a substrate temperature of ~850 °C for 1 h. Deposition was followed by 5 min exposure to a pure H$_2$ plasma to ensure the diamond surface was hydrogen terminated. This resulted in faceted diamond crystallites of size ~1 μm and a film thickness of ~6 μm. Being undoped, the samples were essentially insulating, however measurement of the surface conductivity using 2-point probes gave values ~1 MΩ from surface transfer doping arising from an aqueous adsorbate layer that develops on exposure to air [32].

2.1.2. Undoped nanocrystalline diamond (NCD)

Deposition and hydrogen termination occurred at 20 torr in a hot filament reactor under standard CVD conditions [33], using a rhenium filament (2400 K) positioned 3 mm above the surface of the heated substrate (~900 °C) for 8 h. The gas mixture used was 4%CH$_4$ in H$_2$. This produced rounded crystallites of size ~400 nm and film thickness ~4.5 μm.

2.1.3. Undoped ultrananocrystalline diamond (UNCD)

These samples were deposited and hydrogen-terminated using a microwave plasma CVD (MWCVD) reactor operating at 0.7 kW and 200 Torr, using 0.75%CH$_4$/5.6%H$_2$/Ar process gases at a substrate temperature of ~650 °C, for 2 h. The UNCD samples were ~0.5 μm thick, with a topography that was smooth and consisted

of spherical crystallites of size <10 nm surrounded by an amorphous carbon matrix [34].

2.1.4. Lightly boron-doped MCD

Deposition and hydrogen-termination occurred identically to that described in Section 2.1.1 except with the addition of ~50 ppm of diborane to the gas mixture. This produced samples of the same thickness and indistinguishable in morphology from the undoped MCD samples. The major difference was that these B-doped samples were *p*-type semiconducting with a 2-point resistivity of ~160 kΩ. Prior calibration using SIMS [35] enabled us to estimate the B concentration as ~2.4×10^{19} cm^{-3}.

2.1.5. Heavily boron-doped MCD

These were deposited and hydrogen-terminated as described in Section 2.1.1 except with the addition of ~10,000 ppm of diborane to the gas mixture. This produced blue–black, facetted samples of thickness ~3 μm, with near metallic conductivity (a 2-point resistivity of 100 Ω consistent with a B content of ~9×10^{20} cm^{-3}).

2.1.6. Nitrogen-doped NCD

Deposition occurred in a MWCVD reactor using 6.5%CH$_4$/0.7%N$_2$/H$_2$ at 110 Torr and 1.0 kW to produce N-doped NCD samples. Deposition for 1 h resulted in a film thickness of ~5 μm. The nitrogen content in the gas mixture caused renucleation of the diamond surface leading to a reduction in crystal size and resulting in NCD samples [36]. Although doping with N should make the material *n*-type, most of the incorporated N is passivated by *p*-type defects present at grain boundaries and defect sites. This, together with the high activation energy for N in diamond (1.7 eV) resulted in these samples being resistive, >10 MΩ.

2.1.7. Phosphorus-doped MCD

These films were deposited onto highly resistive (10–20 kΩ cm) Si (1 0 0) substrates using a 5 kW ASTeX PDA-18 MWCVD reactor at Hasselt University in Belgium. The process used 1% CH$_4$/H$_2$ with the addition of PH$_3$ (10,000 ppm P/C) at a pressure of 50 torr and substrate temperature of 820 °C. The resulting 2.5-μm-thick P-doped film exhibited *n*-type semiconductivity with an estimated P content of 1×10^{19} cm^{-3} [31]. The surface was re-hydrogenated immediately prior to PF-TUNA measurements by exposure to a H$_2$ plasma for 5 min.

2.2. PeakForce tunnelling atomic force microscopy (PF-TUNA) investigation

PF-TUNA was performed utilising a Multi-mode VIII AFM with Nanoscope V controller and PF-TUNA module [Bruker, CA, USA] in ambient conditions. Conductive silver paint (G3790 – Agar Scientific) was used to attach the base of the Si substrate to a steel disc and to make electrical contact between this disc and the edges of the diamond films, enabling a bias to be applied between the grounded sample and the AFM tip. Topographic and tunnelling current information were collected under PeakForce feedback – a non-harmonic AFM feedback that oscillates the sample and uses the resulting cantilever-force curves to maintain a set-point force level. Therefore, the interaction force between the conductive tip and the sample can be minimized to the point that tunnelling current measurements are collected with a minimum of 1 nm separation between the tip and the sample. This has the additional benefit of protecting the tip from being damaged by the sample – a crucial factor when investigating a hard sample such as diamond – particularly when scanning large features such as micrometre-sized grains or high r.m.s. roughness. The cantilevers used were PF-TUNA [Bruker, CA, USA] with a nominal spring constant of 0.4 N m^{-1}. A PtIr coating on the tip of the cantilever

allowed the measurement of the tunnelling current when a bias was applied between the tip and the sample, and provided a nominal tip radius of 20 nm (though smaller tip radii have been observed). Precautions were taken to ensure that both the roughness and hardness of the diamond samples did not cause excess wear to the tip and risk damage to the conducting Pt-Ir layer, as previously described in detail [29]. Images were collected at a resolution of 5120 × 5120 pixels at a tip-sample bias of <5 mV and a scan rate of 0.1 Hz to allow maximum dwell time for current measurement. A variety of tests have previously been performed confirming that the measured tunnelling current in this scenario is a true reflection of the emission properties of the surface and not simply an artefact of surface topography [29].

Emission currents measured were in the range of a few pA to a few hundred pA per emission site, with tip-sample biases varying from 1 mV to 1 V. However, the *absolute* scale of measured currents for each film has not been included as they are not directly comparable between samples. This is due to variations in thickness of the Si substrates onto which the diamond films were deposited, and the small variation in resistance of cantilevers, and their tip radii, used to examine each sample. Nevertheless, the physical percentage of the surface emitting electrons per unit area has been calculated to provide a relative comparison of the efficiency of emission between the different diamond films.

3. Results

Fig. 1 shows the emission intensities from the various diamond samples. It is clear that emission intensity depends largely upon two factors, doping level and grain size (or number of grain boundaries). Considering only the undoped samples first, with decreasing grain size, a greater percentage of the diamond surface comprises of grain boundaries. If emission intensity remains constant at a grain boundary independent of the size of the grain then the relative conductivity per unit area should be inversely proportional to the average grain size of the sample. This effect is observed in Fig. 1 where the small amount of emission from undoped MCD (Fig. 1(a)) is irregular and confined to grain boundaries along the edges of individual isolated large crystallites. In comparison, the overall emission from the smaller-grained NCD sample (Fig. 1(e)) is more intense and the grain boundary emission sites have linked together to form a network of interconnected regions. Finally, emission from the UNCD sample (Fig. 1(h)) is uniformly intense over the scanned area from a dense network of emitting grain boundaries.

The emission intensity was quantified by measuring the emission current above a threshold set at the r.m.s. current for each sample, to give an estimate for the percentage of the surface area that emits electrons. The bar-chart in Fig. 1 shows that for the undoped samples the percentage emitting area is inversely proportional to grain size: 18% for MCD, 26% for NCD and 49% for UNCD. The effect of this is shown over large (10 μm × 10 μm) and small (3 μm × 3 μm) regions in Fig. 2 where measured emission current has been overlaid on three-dimensional representations of surface topography as a blue colour-scale. It can clearly be seen that the emission comes from the valleys between the facets, and for smaller-grained samples there is greater emission overall (the image becomes brighter) as the density of emission sites increases.

Turning now to the doped samples, Fig. 1 shows that P-, N-, and B-doped diamond samples all show increased total emission current compared to their undoped counterparts, as expected for samples with higher electrical conductivity. For the B-doped samples, at low (Fig. 1(c)) and high (Fig. 1(d)) doping, 80–90% of the surface emits electrons. Fig. 3 shows the emission current overlaid on surface topography for a lightly B-doped and a heavily B-doped sample. The images show that because the grains have become

significantly more conductive, emission has spread from the grain boundaries to much of the grain facets as well, although the effect is greater on some grain faces than on others. The reason for this is not clear, but it is known that some faces, particularly (1 1 1), contain more defects. Local enhancement of boron content has been found in these grain defects, and the higher order the defect, the more boron it contains [37]. Although the effect is probably small, this may provide an explanation for the very local enhancement of conductivity observed on different faces. The highly B-doped sample, with near metallic conductivity, shows emission uniformly across the surface, *i.e.* from facets and grain boundaries almost equally.

Doping of CVD diamond with phosphorus is somewhat different to boron incorporation. First, the dopant concentration is much lower, and although the samples are nominally *n*-type [37,38] the conductivity remains quite low. There is also a significant difference in the topography. Fig. 4 depicts a P-doped MCD sample with predominantly square-faced (1 0 0) facets in place of randomly oriented ones. These square faces have negligible electron emission, with almost all emission coming from either the grain boundaries or the (1 1 1) side faces. From low-resolution imaging (Fig. 4(a)), it appears that the phosphorus has produced a similar effect to that of boron doping, with different faces of each grain emitting with differing intensities, but with broad emission sites along grain boundaries. Previous work has shown that P-incorporation in microcrystalline diamond films is very sensitive to the actual grain orientation, with local variations of more than one order of magnitude not being uncommon [38]. In Fig. 4(c) higher resolution mapping reveals that the supposedly smooth (1 1 1) side-faces of the P-doped MCD grains are actually composed of a series of densely packed steps separated by small (1 0 0) regions. Electrons are emitted strongly from the boundaries around these steps, leading to a mottled pattern in the PF-TUNA images across the side facets. The density of these step-edges on the (1 1 1) face results in a greater percentage of the surface emitting electrons (62%, from Fig. 1) compared with the undoped MCD sample. Indeed, the percentage of the surface emitting electrons is even greater than that of undoped UNCD (49%).

Fig. 5 shows that addition of nitrogen to the CVD process produces an NCD structure with high-intensity electron emission from what appear to be broad grain-boundary emission sites, similar to that seen in the UNCD sample in Fig. 2(e, f). Even at high resolution, no patterns due to (1 1 1) step edges were observed. Over time, the width of grain-boundary emission sites appeared to decrease, along with the overall relative surface conductivity. This was investigated by measuring the total r.m.s. emission current as a function of time, and the results are shown in Fig. 5 for the N-doped NCD sample. The greatest decrease occurred within the first 25–30 h after the sample was removed from the reactor and exposed to ambient conditions. After this period the sample reached a stable state and the relative surface conductivity remained roughly constant. Multiple areas of the sample were tested and found to have similar surface conductivity within uncertainty. After 805 h the sample was baked at 200 °C in vacuum for 2 h to remove surface adsorbates. This produced an increase in surface conductivity, although the sample did not return to its original higher conductivity value, but instead decreased to the same constant level in a shorter timescale of ∼2.5 h, ten times faster than the original decay. Comparison between Fig. 5(a) and (b) qualitatively suggests that the observed reduction in conductivity is due to the decreasing width of the grain boundary emission sites with time. Fig. 1 shows that N-doped NCD remains overall more conductive than undoped NCD, but that the percentage of the surface emitting electrons decreases from 50% to 41% after exposure to ambient conditions for >30 h, while undoped NCD has 28% of the surface emitting.

4. Discussion and conclusions

The authors emphasise that PF-TUNA measurements are not identical to those in standard field emission experiments, and so interpreting these results must be approached with caution. In standard field emission the tunnelling is from the surface into the vacuum, followed by a relatively long distance flight through vacuum before the electron strikes the electrode/tip. The initial tunnelling is dependent upon the local field strength and not the tip-sample distance — although this effectively sets the local field strength. In PF-TUNA, the tunnelling is direct, from the surface through a 1 nm air–gap into the tip and is, therefore, strongly dependent upon the tip-sample separation. Nevertheless, we propose that the two mechanisms are sufficiently similar that the PF-TUNA measurements can be taken to be representative of preferred field emission sites from polycrystalline diamond surfaces.

Provided this assumption is correct, this work has provided direct evidence that electron field emission from diamond surfaces originates preferentially from the grain boundaries in low conductivity polycrystalline diamond samples, and not from the top of pointed features, sharp edges, or other topographical features. This is consistent with the model for electron field emission based on lowering of the emission threshold due to a reduction of the electron affinity of the diamond surface surrounding graphitic structures on the surface [11], and corroborates the initial findings of ourselves [29] and previous groups [23–25]. As long as the grain boundaries remain relatively conducting compared to the bulk grains, electrons can travel from the contact at the reverse side of the Si substrate into the base of the film, then up the grain boundaries and be emitted at the surface. However, doping changes the situation, because the grains now become conducting allowing some of the current to be transported through the grains themselves and be emitted from the facets. At low B doping levels this is observed as an emitting region creeping up the side of the grains [29], while for low N doping the grain-boundary emission sites are broader. In contrast, at higher B-doping levels, where the grains have near metallic conductivity, both the grains and the grain boundaries emit almost equally, so that the emission is more uniformly distributed over the whole surface.

The story changes again with low P-doping; low-resolution scans suggest that entire grain (1 1 1) surfaces emit uniformly together with the grain boundaries – which according to the above discussion should not happen with such a low conductivity sample. Instead, higher-resolution scans showed that the seemingly even emission from these surfaces is not uniform, but has regions of high emission adjacent to regions of low emission. This is consistent with a description of the (1 1 1) surface that is not perfectly flat but composed of a series of growth terraces separated by ridges. Fig. 6(a, b) show high resolution AFM scans of the surface of the grains, where the growth terraces are clearly visible, while Fig. 6(c) shows a height line-scan across a grain. It is known that P incorporates preferentially into the (1 1 1) surface [39] and its large atomic size relative to C can cause distortions in the lattice. Hence, we postulate that the (1 1 1) surfaces of P-doped diamond crystallites are not as smooth as those in undoped or B-doped diamond, and the high density of ridges provide the necessary surface defects to enhance emission locally, as depicted in Fig. 6(d). Indeed, in the course of preparing samples for this paper, we grew a range of undoped and B-doped films with varying growth conditions and alpha-parameters, but these process changes only really affected the grain size and/or overall crystallite shape. Despite their variation in crystallite size and morphology, nearly all these undoped or B-doped films had facets with relatively smooth (1 0 0) or (1 1 1) faces. Growth of microstepped facets was not impossible under these conditions, just quite rare – unless the concentration

of dopant gas became very large. In contrast, with light P-doping, crystallites with microstepped facets were readily deposited, and we presume this is due to the P atoms preferentially adsorbed on the (1 1 1) faces inhibiting the usual smooth step-flow diamond growth process.

Finally, we have shown that the measured emission current decreases with the time that the sample is exposed to ambient air, and reaches a constant value of ~10% of its initial value after about 30 h. The emission behaviour can be partially recovered following an oven bake, but falls off again with further air exposure. This is consistent with the model for surface transfer doping [32], in which aqueous adsorbates form on the diamond surface, changing its surface conductivity. For the PF-TUNA measurements, the conducting surface layer might cause the localised enhancement in the electric field (and concomitant decrease in the local work function) from the nanoscale grain boundaries to be spread out over a larger area of the surface. Thus, the local field enhancement would be reduced, and the surface would behave as if there were fewer, broader or even no grain boundaries, giving a greatly reduced emission current. Researchers wishing to study field emission from diamond are therefore recommended to make the measurements immediately after sample preparation, or to store the samples under vacuum or inert gas. However, the fact that the emission current does not fully recover after an oven bake suggests that surface transfer doping is not the complete story, and that some irreversible degradation of the surface has also occurred during electron emission. A similar effect was reported by Gan et al. [40]; they found that the surface conductivity of nanocrystalline diamond decreased reversibly after baking at 150 °C due to surface water loss, but irreversibly after baking at temperatures >350 °C. The authors attributed this irreversible change as possibly due to H diffusion and passivation of some dangling bonds in the inter-grain material. In our case, the baking temperature of 200 °C was too low to cause this effect, but may have caused slight loss of H from the surface, sufficient to reduce the surface conductivity.

A final conclusion from this study is that patterning diamond into sharp cones or needles to enhance the field emission is unnecessary. Conducting *n*- or *p*-type diamond samples with a large number of grain boundaries (such as NCD, UNCD or P-doped MCD) provide excellent emission sources, even from a flat surface.

Acknowledgments

Appendix A. Supplementary data

Supplementary data associated with this article can be found, in the online version, at http://dx.doi.org/10.1016/j.carbon.2015.06.082.

References

[1] J.L. Davidson, W.P. Kang, K. Subramanian, Y.M. Wong, Forms and behaviour of vacuum emission electronic devices comprising diamond or other carbon cold cathode emitters, Phil. Trans. R. Soc. A 366 (2008) 281.

[2] K. Subramanian, W.P. Kang, J.L. Davidson, N. Ghosh, K.F. Galloway, A review of recent results on diamond vacuum lateral field emission device operation in radiation environments, Microelectron. Eng. 88 (2011) 2924.

[3] S.V. Baryshev, S. Antipov, J.H. Shao, C.G. Jing, K.J.P. Quintero, J.Q. Qiu, W.M. Liu, W. Gai, A.D. Kanareykin, A.V. Sumant, Planar ultrananocrystalline diamond field emitter in accelerator radio frequency electron injector: Performance metrics, Appl. Phys. Lett. 105 (2014) 203505.

[4] K.J.P. Quintero, S. Natipov, A.V. Sumant, C.G. Jing, S.V. Baryshev, High quantum efficiency ultrananocrystalline diamond photocathode for photoinjector applications, Appl. Phys. Lett. 105 (2014) 123103.

[5] Y. Zou, P.W. May, S.M.C. Vieira, N.A. Fox, Field emission from diamond-coated multiwalled carbon nanotube 'teepee' structures, J. Appl. Phys. 112 (2012) 044903.

[6] G. Chen, S. Neupane, W. Li, L. Chen, J. Zhang, An increase in the field emission from vertically aligned multiwalled carbon nanotubes caused by NH₃ plasma treatment, Carbon 52 (2013) 468.

[7] J.-M. Bonard, M. Croci, I. Arfaoui, O. Noury, D. Sarangi, A. Châtelain, Can we reliably estimate the emission field and field enhancement factor of carbon nanotube film field emitters?, Diamond Relat Mater. 11 (2002) 763.

[8] M. Chhowalla, C. Ducati, N.L. Rupesinghe, K.B.K. Teo, G.A.J. Amaratunga, Field emission from short and stubby vertically aligned carbon nanotubes, Appl. Phys. Lett. 79 (2001) 2079.

[9] C.J. Shearer, J.G. Shapter, J.S. Quinton, P.C. Dastoor, L. Thomsen, K.M. O'Donnell, Highly resilient field emission from aligned single-walled carbon nanotube arrays chemically attached to n-type silicon, J. Mater. Chem. 18 (2008) 5753.

[10] M.W. Geis, N.N. Efremow, K.E. Krohn, J.C. Twichell, T.M. Lyszczarz, R. Kalish, J.A. Greer, M.D. Tabat, A new surface electron-emission mechanism in diamond cathodes, Nature 393 (1998) 431.

[11] J.B. Cui, J. Ristein, M. Stammler, K. Janischowsky, G. Kleber, L. Ley, Hydrogen termination and electron emission from CVD diamond surfaces: a combined secondary electron emission, photoelectron emission microscopy, photoelectron yield, and field emission study, Diamond Relat. Mater. 9 (2000) 1143.

[12] D. Pradhan, I.N. Lin, Grain-size-dependent diamond–nondiamond composite films: characterization and field-emission properties, ACS Appl. Mater. Interfaces 1 (2009) 1444.

[13] J.B. Cui, J. Ristein, L. Ley, Low-threshold electron emission from diamond, Phys. Rev. B 60 (1999) 16135.

[14] J. Robertson, Mechanisms of electron field emission from diamond, diamond-like carbon, and nanostructured carbon, J. Vac. Sci. Technol. B 17 (1999) 659.

[15] A.C. Ilie, A.C. Ferrari, T. Yagi, S.E. Rodil, J. Robertson, E. Barborini, P. Milani, Role of sp² phase in field emission from nanostructured carbons, J. Appl. Phys. 90 (2001) 2024.

[16] J.B. Cui, J. Robertson, Field emission from chemical vapor deposition diamond surface with graphitic patches, J. Vac. Sci. Technol. B 20 (2002) 238.

[17] Y. Miyamoto, T. Miyazaki, D. Takeuchi, H. Okushi, S. Yamasaki, Ab initio dynamics of field emission from diamond surfaces, Appl. Phys. Lett. 103 (2013) 123104.

[18] S.A. Getty, O. Auciello, A.V. Sumant, X. Wang, D.P. Galvin, P.R. Mahaffy, Characterization of nitrogen-incorporated ultrananocrystalline diamond as a robust cold cathode material, in: T. George, M.S. Islam, A.K. Dutta (eds.), Micro- and Nanotechnology Sensors, Systems, and Applications-II, 2010 (Proc. SPIE. 7679: 76791N–1).

[19] P.W. May, S. Höhn, M.N.R. Ashfold, W.N. Wang, N.A. Fox, T.J. Davis, J.W. Steeds, Field emission from chemical vapor deposited diamond and diamond-like carbon films: investigations of surface damage and conduction mechanisms, J. Appl. Phys. 84 (1998) 1618.

[20] J.M. Garguilo, F.A.M. Köck, B. Brown, R.J. Nemanich, Field Emission, PEEM and FEEM Measurements of emitting sites of MPCVD grown nanocrystalline diamond films, in: Proc. Sixth Appl. Diamond Conf./Second Frontier Carbon Technol. Joint Conf., 2001, vol. 133.

[21] A.V. Karabutov, V.D. Frolov, S.M. Pimenov, V.I. Konov, Grain boundary field electron emission from CVD diamond films, Diamond Relat. Mater. 8 (1999) 763.

[22] A.R. Krauss, O. Auciello, M.Q. Ding, D.M. Gruen, Y. Huang, V.V. Zhirnov, E.I. Givargizov, A. Breskin, R. Chechen, E. Shefer, V. Konov, S. Pimenov, A. Karabutov, A. Rakhimov, N. Suetin, Electron field emission for ultrananocrystalline diamond films, J. Appl. Phys. 89 (2001) 2958.

[23] K.J. Sankaran, K. Panda, B. Sundaravel, N.H. Tai, I.N. Lin, Enhancing electrical conductivity and electron field emission properties of ultrananocrystalline diamond films by copper ion implantation and annealing, J. Appl. Phys. 115 (2014) 063701.

[24] K. Panda, K.J. Sankaran, E. Inami, Y. Sugimoto, N.H. Tai, I.N. Lin, Direct observation and mechanism for enhanced field emission sites in platinum ion implanted/post-annealed ultrananocrystalline diamond films, Appl. Phys. Lett. 105 (2014) 163109.

[25] V. Yanev, M. Rommel, M. Lemberger, S. Petersen, B. Amon, T. Erbacher, A.J. Bauer, H. Ryssel, A. Paskaleva, W. Weinreich, et al., Tunneling atomic-force microscopy as a highly sensitive mapping tool for the characterization of film morphology in thin high-k dielectrics, Appl. Phys. Lett. 92 (2008) 252910.

[26] B. Bhushan (Ed.), Springer Handbook of Nanotechnology, 2nd Edition, Springer, Heidelberg, Germany, 2007.

[27] R. Garcia, R. Perez, Dynamic atomic force microscopy methods, Surf. Sci. Rep. 47 (2002) 197.

[28] F.J. Giessibl, S. Hembacher, H. Bielefeldt, J. Mannhart, Subatomic features on the silicon (111)-(7×7) surface observed by atomic force microscopy, Science 289 (5478) (2000) 422.

[29] V. Chatterjee, R.L. Harniman, P.W. May, P.K. Barhai, Direct observation of electron emission from the grain boundaries of chemical vapour deposition

diamond films by tunneling atomic force microscopy, Appl. Phys. Lett. 104 (2014) 171907.

[30] O.J.L. Fox, J.O.P. Holloway, G.M. Fuge, P.W. May, M.N.R. Ashfold, Electrospray deposition of diamond nanoparticle nucleation layers for subsequent CVD diamond growth, in: P. Bergonzo, J.E. Butler, R.B. Jackman, K.P. Loh, M. Nesladek (eds.), Diamond Electronics and Bioelectronics – Fundamentals to Applications III, (Mater. Res. Soc. Symp. Proc. Volume 1203, 2010), paper J17–27.

[31] W. Janssen, S. Turner, G. Sakr, F. Jomard, J. Barjon, G. Degutis, Y.-G. Lu, J. D'Haen, A. Hardy, M. Van Bael, J. Verbeeck, G. Van Tendeloo, K. Haenen, Substitutional phosphorus incorporation in nanocrystalline CVD diamond thin films, Phys. Status Solidi RRL 8 (2014) 705.

[32] P. Strobel, M. Riedel, J. Ristein, L. Ley, Surface transfer doping of diamond, Nature 430 (2004) 439.

[33] P.W. May, Diamond Thin Films: A 21st Century Material, Phil. Trans. R. Soc. Lond. A 358 (2000) 473.

[34] O.J.L. Fox, J. Ma, P.W. May, M.N.R. Ashfold, Yu.A. Mankelevich, The role of inert gas in MW-enhanced plasmas for the deposition of nanocrystalline diamond thin films, Diamond Relat. Mater. 18 (2009) 750.

[35] P.W. May, W.J. Ludlow, M. Hannaway, P.J. Heard, J.A. Smith, K.N. Rosser, Raman and conductivity studies of boron doped microcrystalline diamond, facetted nanocrystalline diamond and cauliflower diamond films, Diamond Relat. Mater. 17 (2008) 105.

[36] A.J. Eccles, T.A. Steele, A. Afzal, C.A. Rego, W. Ahmed, P.W. May, S.M. Leeds, Influence of B- and N-doping levels on the quality and morphology of CVD diamond, Thin Solid Films 343–344 (1999) 627.

[37] Y.-G. Lu, S. Turner, J. Verbeeck, S.D. Janssens, P. Wagner, K. Haenen, G. Van Tendeloo, Direct visualization of boron dopant distribution and coordination in individual chemical vapor deposition nanocrystalline B-doped diamond grains, Appl. Phys. Lett. 101 (4) (2012) 041907.

[38] K. Haenen, A. Lazea, J. Barjon, J. D'Haen, N. Habka, T. Teraji, S. Koizumi, V. Mortet, P-doped diamond grown on (110)-textured microcrystalline diamond: growth, characterization and devices, J. Phys. Cond. Matter 21 (36) (2009) 364204.

[39] S. Koizumi, M. Kamo, Y. Sato, H. Ozaki, T. Inuzuka, Growth and characterization of phosphorous doped 111 homoepitaxial diamond thin films, Appl. Phys. Lett. 71 (1997) 1065.

[40] L. Gan, A. Bolker, C. Saguy, R. Kalish, D.L. Tan, B.K. Tay, D. Gruen, P. Bruno, The effect of grain boundaries and adsorbates on the electrical properties of hydrogenated ultra nano crystalline diamond, Diamond Relat. Mater. 18 (2009) 1118.